Resonant manifold multiplexers

Yu, Yang; Wang, Yi; Guo, Cheng; Cheng, Qingsha S.; Yu, Ming

DOI:
10.1109/TMTT.2021.3120450

Resonant Manifold Multiplexers

Yang Yu, *Student Member, IEEE*, Yi Wang, *Senior Member, IEEE*, Cheng Guo, Qingsha S. Cheng, *Senior Member, IEEE* and Ming Yu, *Fellow, IEEE*

***Abstract*—This article presents a new compact multiplexer structure and its design approach, based on a novel resonant manifold. Different from typical transmission-line based manifold multiplexers, the proposed manifold junction is formed of coupled-resonators, so that the manifold also contributes to the filtering poles and selectivity in the passbands. The all-resonator configuration achieves a more compact footprint than the conventional manifold. This multi-port filtering network can be represented by a single coupling matrix which can be obtained by using a robust optimization-based method. Tailored channel frequency allocation schemes are presented for the proposed multiplexers with a different number of channels. To validate the proposed concept, a triplexer and a 5-channel multiplexer, both at X-band, are designed and tested using rectangular waveguide technology. Good agreements have been achieved between the measurement and simulations. Comparisons have been made with conventional multiplexers.**

***Index Terms*—All-resonator structure, coupling matrix theory microwave multiplexers, manifold multiplexers, optimization, step tune method.**

I. Introduction

MICROWAVE multiplexers are widely employed components in communication systems such as satellite payloads and cellular base stations [1]-[3]. They are used for filtering as well as frequency distribution. A wideband signal is separated into several narrowband channels or vice versa [1]. The output multiplexer (OMUX) in satellite payloads often handles high-power, so maintaining low insertion losses is very important [4]. This usually requires the use of waveguide technology [5].

There have been several configurations used to implement the multiplexers [2]. Some configurations combine hybrids or circulators with channel filters to simplify design and tuning as well as to improve the isolation performance between channels [2]. However, these configurations lead to relatively high losses and large footprints due to the use of hybrids and circulators [2]-[3], [5]. To make the signal distribution network in multiplexes more compact, manifold-junction and star-junction configurations were developed and eventually became the mainstream [2], [5]. The star-junction multiplexers combine all the channel filters to a resonant or a non-resonant node. A coupling matrix representing the multiplexer can be systematically obtained based on the calculated characteristic polynomials of the multiplexer [2], [6]. The multiplexers are physically realized based on the obtained coupling matrix and have been applied in base station applications for mobile communications [2], [6]-[8].

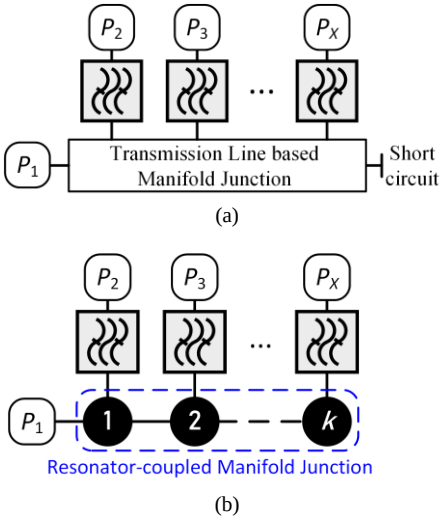

Fig. 1. (a) Schematic diagram of a conventional manifold multiplexers; (b) Schematic diagram of the proposed resonant manifold multiplexer.

Manifold multiplexers are usually designed using optimization-based methods rather than synthesis-based approaches [5], [9]. In a typical manifold multiplexer, as illustrated in Fig. 1(a), multiple channel filters are connected with a transmission-line-based manifold junction (normally a waveguide) with optimized separations between them [3]. There exists relatively strong interaction between each channel filter, comparing with those using hybrids or circulators. The manifold has to be integrally designed to compensate for the mutual influence between channels [3]. This also means any change in frequency allocation of channels will require a new multiplexer design [3]. Furthermore, as the number of channels increases, a greater number of variables have to be considered at the same time and the large volume of the component also increases the difficulty in EM simulations and optimization [5]. There have been many contributions to tackle the optimization problems [2], [5], [8]. A "diakoptics" approach is generally taken. This involves segmenting the whole network into sub-elements, full-wave EM simulation of the sub-elements

Manuscript received March 2nd, 2021; revised Jun 1st , 2021. (Corresponding author: Y. Wang and Q. S. Cheng.)

This work is partially supported by the UK Engineering and Physical Science Research Council under grant EP/S013113/1 and EP/M013529/1, and by the National Natural Science Foundation of China Grant 62071211 and the University Key Research Project of Guangdong Province under Grant 2018KZDXM063.

Y. Yu, Q. S. Cheng and M. Yu are with the Department of Electrical and Electronic Engineering, Southern University of Science and Technology, Shenzhen, 518055, P.R. China. (emails: issacyu@live.cn, chengqs@sustech.edu.cn, and ming.yu@ieee.org).

Y. Yu and Y. Wang are with the Department of Electrical, Electronic and Systems Engineering, University of Birmingham, Birmingham B15 2TT, U.K. (e-mail: yxy726@student.bham.ac.uk, y.wang.1@bham.ac.uk).

C. Guo is with the Department of Inf. and Communication Engineering, Xi'an Jiaotong University, Xi'an, Shaanxi 710049, China. (email: spmguo@163.com).|

and combining them back into a circuit network to represent the whole structure [10]. For example, using space mapping technique, each channel can be represented by a circuit model and then the multiplexer is optimized channel by channel replacing the circuit model of each channel with the corresponding EM model [11]-[14]. In [5], a low-order EM distributed model, a halfway between an analytical model and a full-wave EM model, was used to leverage the optimization challenges. It provided a good initial design for the full-wave optimization.

An all-resonator-based configuration has also been applied to design multiplexers [15]. The coupled-resonator network is divided into a stem and multiple branches, where resonators can be flexibly assigned according to specification. Such multiplexers are designed based on coupling matrix theory [16]-[21]. A tree topology [15] is usually used in order to minimize the number of couplings associated with each resonator to no more than three. However, the intricate frequency distribution network makes it difficult to be synthesized when the number of channels is larger than four [23].

This paper proposes a new multiplexer configuration using a novel resonant manifold structure based exclusively on coupled resonators. The topology is shown in Fig. 1(b). The transmission-line-based junction is eliminated, while all the resonators in the 'resonant manifold' become an integrated part of the channel filters and they all contribute to the transmission poles and therefore frequency selectivity. The integral coupling configuration can be represented by a single integral coupling matrix. The acquisition of the matrix will be discussed in detail. A tailored channel frequency allocation method is presented to address the difficulty in coupling matrix optimization. The proposed multiplexer is designed by dimensioning using the coupling matrix theory. To tackle the extensive EM optimization tasks, a step-tune method is implemented. To validate the proposed multiplexer structure and design methodology, two exemplary prototypes, a triplexer and a 5-channel multiplexer, are synthesized, designed, and fabricated.

The rest of this paper is organized as follows. Section II introduces coupling matrix for resonant manifold multiplexers. The synthesis and design procedures of the triplexer and the 5-channel multiplexer are discussed in Section III and Section IV, respectively. The fabrication and measurement results of the two multiplexers are presented in Section V. Section VI concludes the paper.

II. Coupling Matrix for Resonant Manifold Multiplexers

The coupling matrix synthesis for the resonant manifold multiplexer is conducted in a normalized frequency domain [2]. As a multi-port resonator-coupled network, the resonant manifold multiplexers can be represented by a single coupling matrix in a block matrix form as [23]

$$\boldsymbol{M} = \begin{bmatrix} \boldsymbol{m} & \boldsymbol{m}_p \\ \boldsymbol{m}_p^T & \boldsymbol{m}_x \end{bmatrix}. \tag{1}$$

Assume that n denotes the number of resonators and X is the number of ports. $\boldsymbol{m}$ is an $n \times n$ submatrix comprising the mutual coupling coefficients $m(i, j)$ denoting a coupling between the ith and the jth resonator ($i \neq j$, $i, j = 1, 2, \ldots, n$), and the self-coupling $m(i, i)$ determining the resonant frequency of the ith resonator. $\boldsymbol{m}_p$ is an $n \times X$ submatrix of input/output couplings, $m(i, p)$ ($p = 1, 2, \ldots, X$). $\boldsymbol{m}_x$ is a $X \times X$ submatrix of couplings between ports and it is normally a zero matrix. Accordingly, the immittance matrix $\boldsymbol{A}$ is given by [24]

$$\boldsymbol{A} = \boldsymbol{R} + s \cdot \boldsymbol{U} - j\boldsymbol{M} \tag{2}$$

where s is a complex normalized frequency variable. $\boldsymbol{R}$ and $\boldsymbol{U}$ are two block matrices defined by

$$\boldsymbol{R} = \begin{bmatrix} \boldsymbol{0} & \boldsymbol{0} \\ \boldsymbol{0} & \boldsymbol{r} \end{bmatrix}, \boldsymbol{U} = \begin{bmatrix} \boldsymbol{u} & \boldsymbol{0} \\ \boldsymbol{0} & \boldsymbol{0} \end{bmatrix} \tag{3}$$

where $\boldsymbol{u}$ and $\boldsymbol{r}$ are identity matrices of the order $n \times n$ and $X \times X$, respectively. The S-parameters, derived from the immittance matrix $\boldsymbol{A}$, are calculated by [23]

$$S_{pp} = \pm\left(1 - 2\boldsymbol{A}^{-1}(p, p)\right) \tag{4}$$

$$S_{pq} = 2 \cdot \boldsymbol{A}^{-1}(p, q) \tag{5}$$

where $\boldsymbol{A}(p, p)$ is the immittance coefficients related to the port p and $\boldsymbol{A}(p, q)$is the immittance coefficient between the port p and q ($p, q = 1, 2, \ldots, X$). S_{pp} is the reflection coefficient at the port p, and S_{pq} is the transmission coefficient between the port p and q.

Since it is difficult to analytically calculate the characteristic polynomials (used to calculate the coupling matrix) for an all-resonator multiplexer, the synthesis generally relies on optimization techniques [21]-[23]. In [23], a systematic optimization-based synthesis approach (so-called GACMS method) was proposed for all-resonator multiplexers. The method hybridizes the filter design knowledge and a robust global optimizer, which combines sequential quadratic programming (SQP) method and self-adaptive differential-evolution optimization technique. This method is capable of dealing with a wide range of diplexer and multiplexer topologies. This method is also employed in this paper.

After coupling matrix synthesis, the normalized coupling matrix will be transformed into the real frequency domain. The mutual couplings $\boldsymbol{m}(i, j)$ and input/output couplings $\boldsymbol{m}_p$ are denormalized by [17]

$$\boldsymbol{M}(i, j) = \boldsymbol{m}(i, j) \cdot FBW \tag{6}$$

$$\boldsymbol{M}_p = \boldsymbol{m}_p \cdot \sqrt{FBW} \tag{7}$$

where FBW is the fractional bandwidth of the multiplexer, $\boldsymbol{M}(i, j)$ and $\boldsymbol{M}_p$ are the couplings in the real frequency domain. The resonant frequency f_i of the ith asynchronously tuned resonator can be calculated with [30]

$$f_i = f_0 \left[\left(\frac{m(i,i) \cdot FBW}{2} \right) - \sqrt{1 + \left(\frac{m(i,i) \cdot FBW}{2} \right)^2} \right] \tag{8}$$

where f_0 is the centre frequency of the multiplexer. With all the

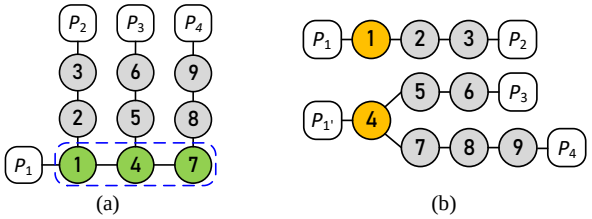

Fig. 2. (a) Coupling topology of the resonant manifold triplexer, where the green circles indicate the resonant manifold. (b)The segment scheme for the triplexer. The synthesis results for the subcircuits are employed as the initial coupling values for the triplexer synthesis.

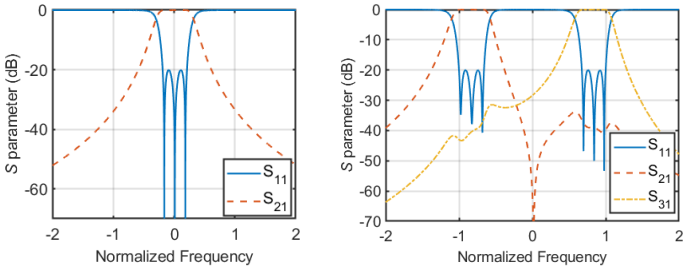

Fig. 3. The S-parameter corresponding to the coupling coefficients of the filter and the diplexer in Fig. 2(b), used as the initial values for the triplexer.

coupling coefficients for the real frequency domain, the physical dimensioning can be executed based on the classical procedure [24]-[25].

III. Resonant Manifold Triplexer

We will first use a triplexer to demonstrate the synthesis of the coupling matrix and the design. The topology of the triplexer with a 3-rd order resonant manifold (Resonator-1, 4 and 7) is shown in Fig. 2(a). Frequency channels are at 9.7 - 9.8 GHz (Channel 1), 9.95 - 10.05 GHz (Channel 2), and 10.2 - 10.3 GHz (Channel 3), respectively. Return loss levels (*RLL*s) of passbands are at 20 dB. The coupling matrix is first obtained with an appropriate channel frequency allocation. Then, the physical dimensioning is implemented according to the obtained coupling matrix. Finally, the multiplexer is optimized starting from the initial dimensions. The details of the design procedure are as follows.

A. Coupling matrix synthesis

To begin with, the passbands are normalized to CH_1: [−1, −0.5919], CH_2: [−0.1879, 0.2119], and CH_3: [0.6079, 1]. For the effective use of the GACMS method, high-quality starting values of the matrix and a reasonable channel frequency allocation are desired. Triplexer segmenting is first conducted to generate the starting coupling coefficients for the triplexer.

In the resonant manifold shown in Fig. 2(a), the junction resonators (Resonator-1 and 4) are the basic frequency distribution elements. By segment of the connection between the two junction resonators1 and 4, as shown in Fig. 2(b), the triplexer is divided into a filter and a diplexer. The starting coupling values for the triplexer come from the synthesis of a filter (Resonator 1 to 3) and a diplexer (Resonator 4 to 9).

For the proposed resonant multiplexer, there are various ways to allocate frequencies to the channels. For this triplexer, there can be six different frequency allocation schemes as illustrated in the Appendix. But not all lead to satisfactory responses. One is chosen for the design, where CH_2, CH_1, and CH_3 are sequentially assigned to the three branches of the triplexer. This is the Scheme 2 shown in the Appendix. The synthesis approach is illustrated in the following.

The starting coupling coefficients are taken from the 3rd-order filter and the 6th-order diplexer with the responses shown in Fig. 3. Optimization on the coupling matrix of the triplexer is then executed using a method similar to [23]. The S-parameter-based objective function is formulated as

TABLE I
THE OPTIMAL COUPLING COEFFICIENTS FOR THE TRIPLEXER

Mutual Couplings	Values	Self-couplings	Values
m(1, 2)	0.2982	*m*(1, 1)	0.0042
m(2, 3)	0.1706	*m*(2, 2)	0.0138
m(1, 4)	0.7113	*m*(3, 3)	0.0138
m(4, 5)	0.2346	*m*(4, 4)	−0.0127
m(5, 6)	0.1780	*m*(5, 5)	−0.7970
m(4, 7)	0.5616	*m*(6, 6)	−0.8240
m(7, 8)	0.2957	*m*(7, 7)	0.1533
m(8, 9)	0.1838	*m*(8, 8)	0.7163
		m(9, 9)	0.8154
Input/output Couplings	**Values**		
m(1, *P*1)	0.7662		
m(3, *P*2)	0.4424		
m(6, *P*3)	0.4478		
m(9, *P*4)	0.4368		

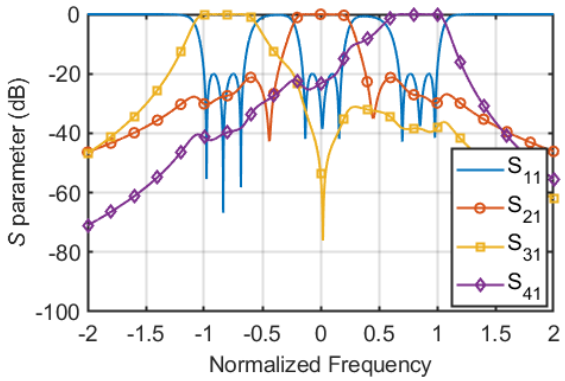

Fig. 4. The S-parameter responses corresponding to the optimized coupling coefficients for the triplexer.

$$O_1 = \frac{\max(PB_1 - (-20), 0)}{20} + \frac{\max(PB_2 - (-20), 0)}{20} + \frac{\max(PB_3 - (-20), 0)}{20} \quad (9)$$

where $PB_1 = \max(|S_{11}(CH_1)|)$; $PB_2 = \max(|S_{11}(CH_2)|)$ and $PB_3 = \max(|S_{11}(CH_3)|)$. Note that for all the frequency allocation schemes are shown in Appendix, the same objective function (9) is utilized. The obtained optimal coupling coefficients are listed in Table I and the corresponding S-parameter responses for the triplexer are shown in Fig. 4. It can be seen that transmission zeros are generated in S_{21} and S_{31}. This is because the resonator 4 and 7 can be seen as two frequency attenuation structures for Channel 1 whereas the resonator 7 is an attenuation structure

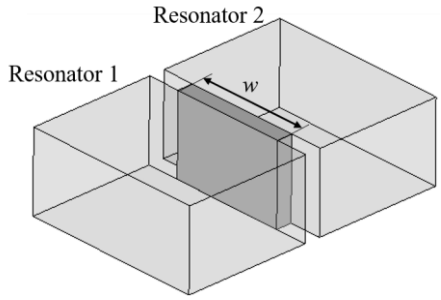

Fig. 5. Structure used to extract the coupling between two waveguide resonators.

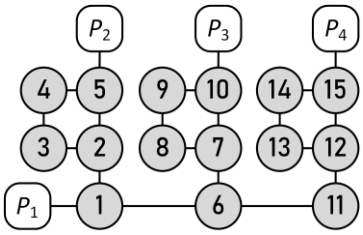

Fig. 6. The coupling topology of the Ku-band triplexer with contiguous channels.

TABLE II
COUPLING COEFFICIENTS FOR THE TRIPLEXER WITH CONTIGUOUS CHANNELS

Mutual couplings					
m(1,2)	0.4809	m(6,7)	0.2904	m(11,12)	0.2821
m(2,3)	0.1874	m(7,8)	0.1867	m(12,13)	0.1850
m(3,4)	0.2162	m(8,9)	0.2312	m(13,14)	0.2282
m(4,5)	0.2656	m(9,10)	0.2811	m(14,15)	0.2786
m(2,5)	-0.0444	m(7,10)	-0.0445	m(12,15)	-0.0443
m(1,6)	0.6684	m(6,11)	0.6404		
Self couplings					
m(1,1)	0.0022	m(6,6)	0.0065	m(11,11)	0.1268
m(2,2)	0.0031	m(7,7)	-0.6667	m(12,12)	0.6430
m(3,3)	0.0036	m(8,8)	-0.6811	m(13,13)	0.6753
m(4,4)	0.0059	m(9,9)	-0.6732	m(14,14)	0.6726
m(5,5)	0.0081	m(10,10)	-0.6742	m(15,15)	0.6597
Input/output Couplings					
m(1, *P*1)	0.9933	*m*(3, *P*2)	0.5812	*m*(6, *P*3)	0.5812
m(9, *P*4)	0.5812				

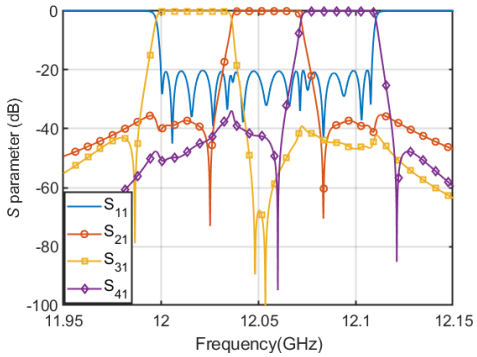

Fig. 7. The S-parameter responses of the contiguous-channel triplexer calculated from the coupling matrix.

for the Channel 2 [26].

It is worth noting that the mutual coupling values within the resonant manifold junction are much larger than those in the branches, as they are required to allow the subsequent channels to pass through. The maximum realizable coupling limits the overall bandwidth the resonant manifold structure can render. Typically coupling matrix used in the synthesis is considered for a narrowband network, i.e., normally less than 20% in fractional bandwidth [31]. The overall bandwidth of the two examples given in this paper is much smaller than this.

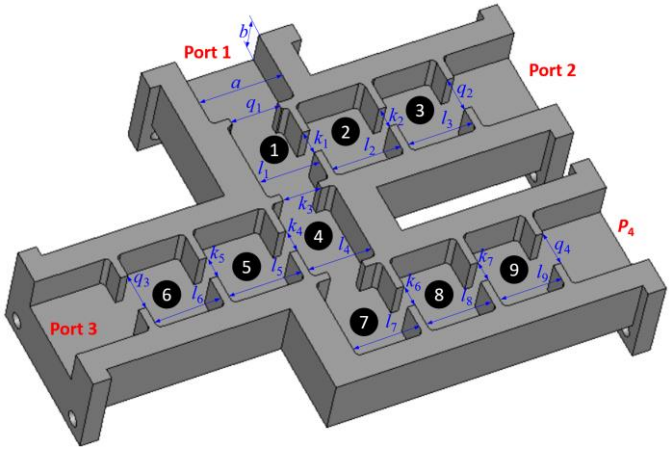

Fig. 8. Configuration of the 9th-order X-band triplexer. a = 22.86, b =10.16, l_1 = 16.70, l_2 = 18.72, l_3 = 17.72, l_4 = 17.30, l_5 = 19.60, l_6 = 18.27, l_7 = 18.00, l_8 = 18.09, l_9 = 16.89, d_1 = 6.43, d_2 = 5.53, d_3 = 10.46, d_4 = 6.10, d_5 = 5.87, d_6 = 9.43, d_7 = 5.84, d_8 = 5.44, q_1 = 13.39, q_2 = 9.43, q_3 = 10.05, q_4 = 9.45. Unit: millimeters. The thicknesses of all the irises are 2 mm. The radiuses of all the blended corners are 1.2 mm.

As a thought experiment, if we scale the triplexer to have a fractional bandwidth of 20%, the largest coupling value required would be m(1,4) = 0.7113 in the normalized frequency domain. The coupling M(1,4) in the real frequency domain will be 0.1423. To achieve this coupling between two X-band rectangular waveguide resonators, as shown in Fig. 5, the width of the coupling window would be about 16.154 mm (out of the broad wall width of 22.86 mm). This is still feasible for X band but starting to approach the limit. In short, it is possible to increase the overall bandwidth of the resonant manifold multiplexer, but the maximum allowable coupling in the resonant manifold structure is the limiting factor.

In the triplexer example, the guard bands between channels are comparable to the channel bandwidth. The developed approach can also obtain the coupling matrix of the multiplexers with contiguous-channels or other complex channel configurations. A Ku-band triplexer is illustrated as an example in Fig. 6, using cascaded quadruplets in the channel filters. The passbands are from 12 GHz to 12.108 GHz and each channel is 36 MHz. Using the same synthesis procedure, the obtained coupling values are listed in Table II and the S-parameter responses are shown in Fig. 7. The synthesis procedure developed in this work is robust and effective enough to generate coupling matrices for resonant manifold multiplexers with complex filtering structures.

B. Physical realization of the 9th-order triplexer

Physical realization is implemented using the denormalized coupling values and resonant frequencies obtained from (6)-(8) [25]. The triplexer is designed based on X-band waveguide technology. The structural configuration is shown in Fig. 8. All the resonators are coupled via inductive irises. The triplexer is

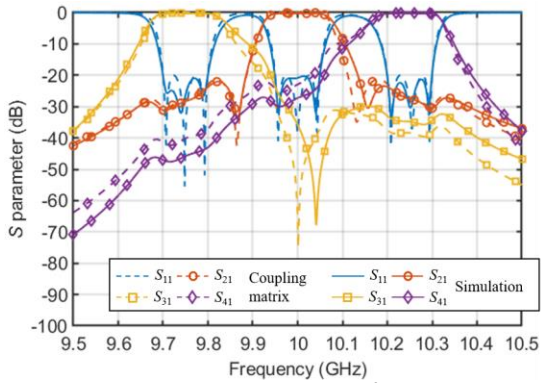

Fig. 9. Simulated S-parameter responses of the 9th-order waveguide triplexer comparing with the ideal S-parameter responses from coupling matrix.

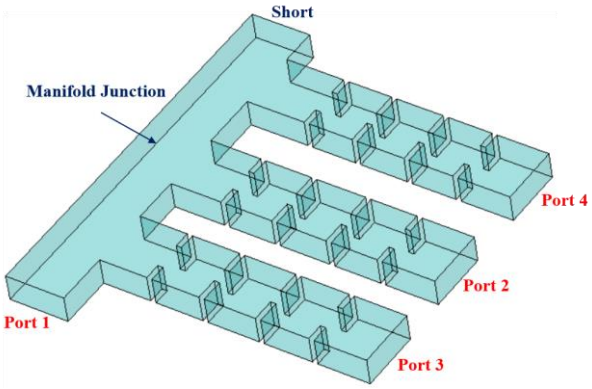

Fig. 10. Air cavity model of a conventional waveguide manifold triplexer.

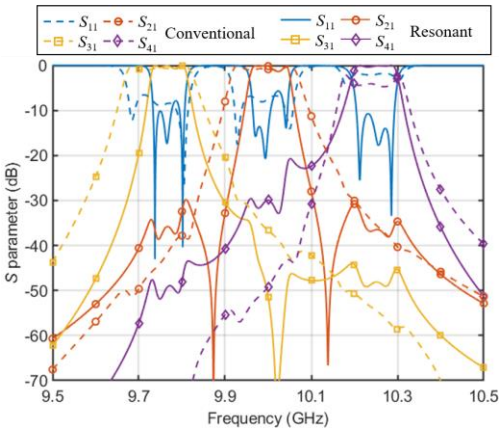

Fig. 11. The starting responses in the design of the two types of triplexers.

optimized using CST Studio Suite [27]. The optimized dimensions are given in Fig. 8. Fig. 9 shows the simulated responses of the 9th-order waveguide triplexer in comparison with those from the coupling matrix. Very good agreement between them has been achieved.

To objectively evaluate the resonant manifold multiplexer, a conventional waveguide manifold multiplexer is designed for comparison, with the same order filtering responses and using the method in [1]. Fig. 10 shows the air-cavity model of the multiplexer where the manifold junction is a standard waveguide. Channel filters are connected to the manifold with intervals of about $\lambda_g/2$, where λ_g is the guided wavelength. Comparing the occupied area of the air cavity (including cavity

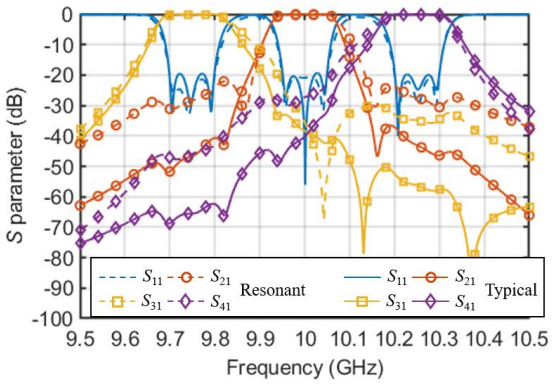

(a)

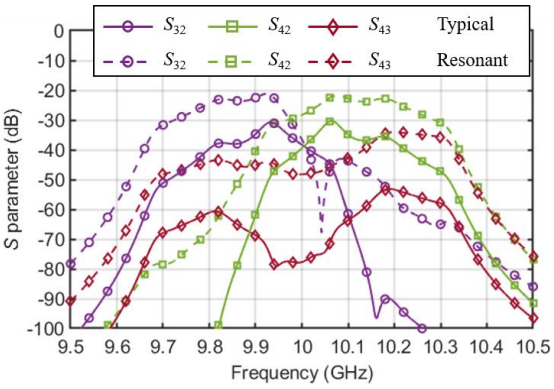

(b)

Fig. 12. Comparison of S-parameter responses between the two types of triplexer configurations. (a) Reflection and transmission; (b) Isolation.

TABLE III
COMPARISONS BETWEEN TWO TYPES OF MANIFOLD MULTIPLEXERS

Type	max($\|S_{11}\|$)	max($\|S_{32}\|$)	max($\|S_{42}\|$)	max($\|S_{43}\|$)	Occupied area
Resonant	−20dB	−21.19dB	−34.02dB	−21.77dB	42cm^2
Typical	−20dB	−30.85dB	−53.32dB	−30.61dB	84cm^2

resonator, manifold junction and coupling irises), this traditional multiplexer takes 84 cm^2, whereas the resonant manifold multiplexer only takes half of the area of 42 cm^2.

The optimization of multiplexers is usually difficult and time-consuming, especially when the number of channels and resonators is large. The design of the resonant manifold multiplexer follows a different routine from the conventional manifold multiplexer. For the latter, the design normally starts from the channel filters and they are then connected together and optimised. The design of the channel filter can provide a reasonable starting point for the multiplexer optimization, but it cannot guarantee the quality of the starting responses. The optimization is still complicated since a large number of EM optimizations are needed [1], [11]-[14]. For the resonant manifold multiplexers, the interaction between channels is much stronger than the conventional one. This presents a challenge to optimization. Direct optimization on the resonant manifold would be more difficult than that on the conventional structure. However, the resonant manifold multiplexer can be designed from a single coupling matrix. Physical dimensioning can be implemented using the coupling extraction method widely adopted in filters [24]-[25]. The physical dimensions

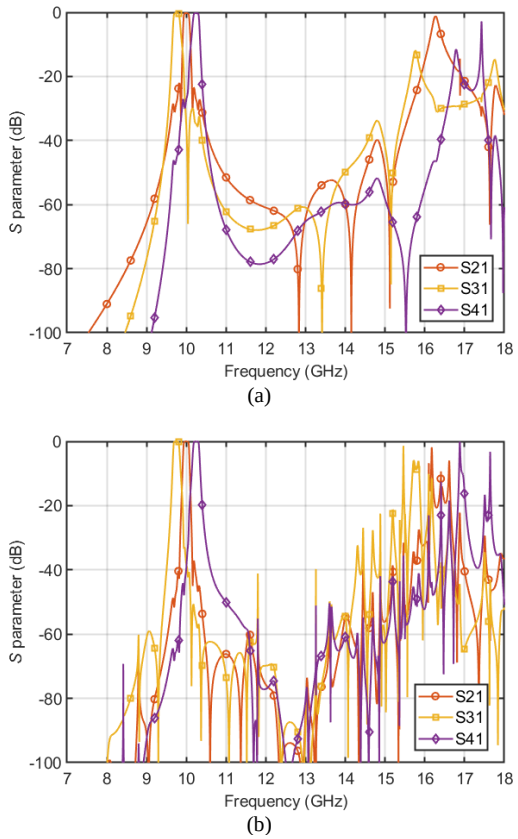

Fig. 13. Out-of-band spurious performance of: (a) The resonant manifold triplexer, (b) The conventional manifold triplexer.

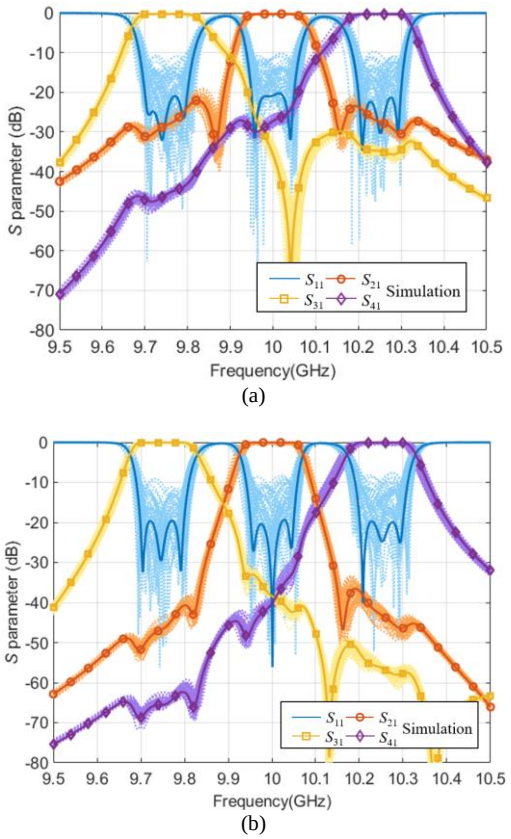

Fig. 14. Tolerance analysis of the two triplexers. (a) Resonant manifold triplexer. (b) Conventional manifold triplexer.

can provide a high-quality initial design for the subsequent optimization. Fig. 11. shows the comparison of the initial design between the two types of triplexers. It can be noticed that the initial S-parameters of the resonant manifold triplexer, extracted using the coupling matrix, can be better than those of the initial design of the conventional one. Furthermore, the coupling matrix can be used to guide the optimization. In this paper, a simple but robust optimization routine called step tuning method [28]-[29], is used. The optimization is effective and fast. The optimization is executed by manually controlling the CST Studio Suite. This process would be accelerated if this can be fully automatic.

Fig. 12 shows the response comparison between two types of manifold multiplexers. As Fig. 12(a) shows, their reflection coefficients are very similar. However, the transmission selectivity of the manifold multiplexer is not as good as that of the traditional manifold. This is mainly caused by the increased interaction between channels through direct couplings. This also results in the 10 dB poorer isolation performance (S_{32}, S_{34} and S_{24} in Fig. 12(b)) of the resonant manifold than the traditional one. Table III compares the performance of the two types of multiplexers.

Fig. 13 compares the out-of-band spurious performance of the two manifold triplexers. It can be observed the resonant manifold triplexer has a clearer harmonic response. Its out-of-band spurious response is at least not inferior to, if not better than, the conventional manifold design used in this work.

We also investigated the two triplexers' sensitivities to fabrication tolerance. This is evaluated using Monte Carlo sampling (MCS) method [32]-[33]. In this analysis, the resonant manifold triplexer has 21 parameters including the dimensions of all the coupling irises and resonator lengths while the conventional one has 27 parameters including the dimensions of coupling iris, resonator lengths and waveguide section lengths in the manifold junction. The manufacturing tolerance is assumed to be ±50 μm. The sampling number is 500 for each triplexer with uniformly random distributed dimensions. 50 curves of each triplexer are random selected to be compared as shown in Fig. 14. As expected, both triplexers are sensitive to the manufacturing tolerance. Seen from the return loss level, the resonant manifold triplexer is slightly less sensitive to the tolerance than the conventional design used in this paper. However, they have similar bandwidth performance. From this comparison, it can be noticed that the resonant manifold triplexer is not more sensitive to dimensional tolerance than the conventional design. Instead, the variation of the manifold dimensions in the conventional manifold seems to have more pronounced effect on the performance. It should be noted that the structure of the conventional manifold used here could be optimized further. We do not intend to generalize the conclusion from this specific comparison. If we were to tune the resonant manifold multiplexer with screws, we expect to face similar challenge as with conventional multiplexer tuning.

IV. Resonant Manifold Pentaplexer

More channels can be designed and implemented using a similar approach. Here a 5-channel resonant manifold

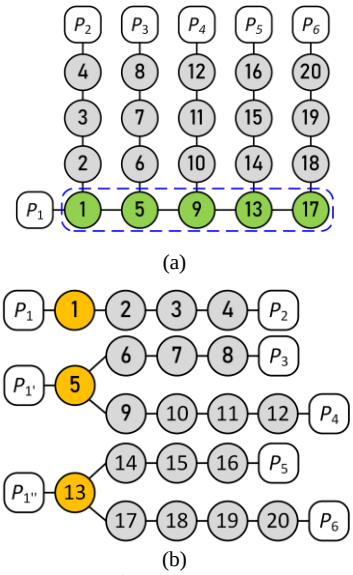

Fig. 15. (a) Coupling topology of the 5-channel resonant manifold multiplexer. (b) The separation scheme for the multiplexer. Sub-circuits are used to find the initial coupling values of the multiplexer.

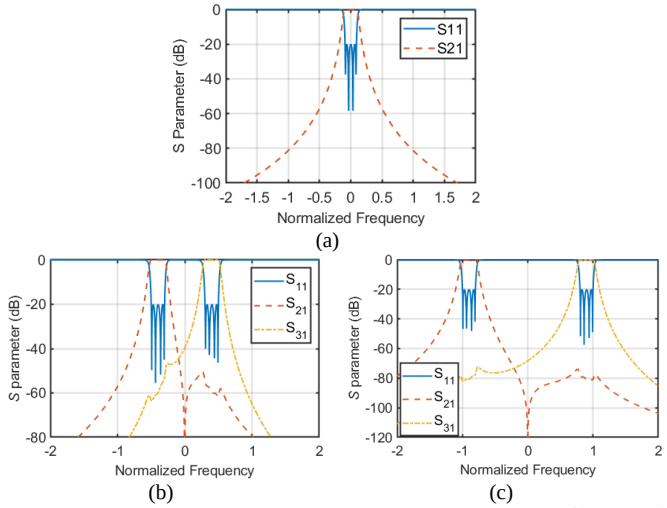

Fig. 16. S-parameter responses corresponding to the coupling coefficients of the sub-circuits in Fig. 9(b).

multiplexer is demonstrated. The coupling topology of the multiplexer is shown in Fig. 15. It consists of 20 coupled resonators wherein resonators 1, 5, 9, 13, and 17 (marked in green) constitute the resonant manifold. The channels are specified as CH_1: 9.55 - 9.65 GHz; CH_2: 9.85-9.95 GHz; CH_3: 10.05 - 10.15 GHz; CH_4: 10.25 - 10.35 GHz; and CH_5: 10.55 - 10.65 GHz. The return losses for all the channels are designed to be larger than 20 dB.

A. Coupling Matrix Synthesis

The normalized passbands are: CH_1: (−1, −0.8088), CH_2: (−0.4324, −0.2471), CH_3: (−0.0638, 0.1178), CH_4: (0.2976, 0.4756), and CH_5: (0.8268, 1). The larger number of channels and coupling coefficients present a great challenge to coupling matrix optimization. High-quality starting values with a suitable frequency allocation scheme are required to facilitate the optimization. Inspired by the successful implementation of the triplexer, the 5-channel multiplexer is divided into a filter

TABLE IV
OPTIMIZED COUPLING COEFFICIENTS FOR THE 5-CHANNEL MULTIPLEXER

Mutual Couplings	Values	Self-couplings	Values
$m(1, 2)$	0.1820	$m(1, 1)$	−0.0060
$m(2, 3)$	0.0601	$m(2, 2)$	0.0220
$m(3, 4)$	0.0794	$m(3, 3)$	0.0219
$m(1, 5)$	0.6640	$m(4, 4)$	0.0215
$m(5, 6)$	0.1284	$m(5, 5)$	−0.0074
$m(6, 7)$	0.0670	$m(6, 6)$	−0.8976
$m(7, 8)$	0.0869	$m(7, 7)$	−0.9041
$m(5, 9)$	0.6081	$m(8, 8)$	−0.9040
$m(9, 10)$	0.1305	$m(9, 9)$	0.0521
$m(10, 11)$	0.0619	$m(10, 10)$	0.8941
$m(11, 12)$	0.0800	$m(11, 11)$	0.9108
$m(9, 13)$	0.3979	$m(12, 12)$	0.9117
$m(13, 14)$	0.1231	$m(13, 13)$	0.0237
$m(14, 15)$	0.0670	$m(14, 14)$	−0.3300
$m(15, 16)$	0.0847	$m(15, 15)$	−0.3390
$m(13, 17)$	0.2817	$m(16, 16)$	−0.3366
$m(17, 18)$	0.1348	$m(17, 17)$	0.0882
$m(18, 19)$	0.0683	$m(18, 18)$	0.3383
$m(19, 20)$	0.0823	$m(19, 19)$	0.3804
		$m(20, 20)$	0.3855
Input/output Couplings	**Values**		
$m(1, P1)$	0.6987		
$m(4, P2)$	0.3122		
$m(8, P3)$	0.3204		
$m(12, P4)$	0.3049		
$m(16, P5)$	0.3154		
$m(20, P6)$	0.3092		

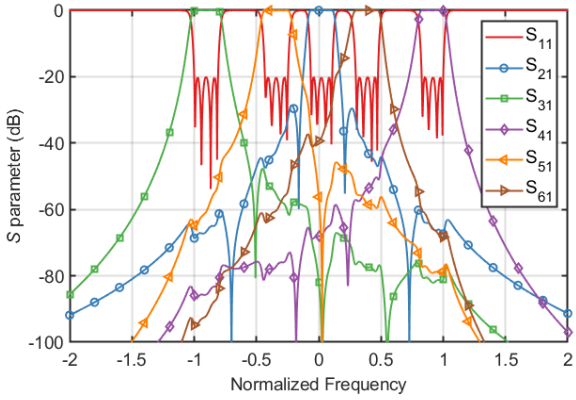

Fig. 17. Calculated S-parameter responses corresponding to the optimized coupling matrix for the 5-channel multiplexer.

and two diplexers, by splitting the coupling $m(1, 5)$ and $m(9, 13)$ between junction resonators as shown in Fig. 15(b). Similarly, as for the channel frequency allocation, the first filter occupies the center channel, namely Channel 3 (−0.0638, 0.1178). The two diplexers occupy the rest of the four channels. Diplexer 1 takes up Channel 1 and 5, while Diplexer 2 takes Channel 2 and 4. The coupling matrices of these three sub-circuits are first synthesized, as shown in Fig. 16, and used to form the initial matrix for the 5-channel multiplexer. This matrix is also optimized using the GACMS method [23]. The optimization goal only contains the passband constraints similar to (9). Since there are a large number of coupling coefficients, group by group optimization is employed in GACMS. Each variable group contains the coupling coefficients related to the initial coupling values of each diplexer. The convergence time is

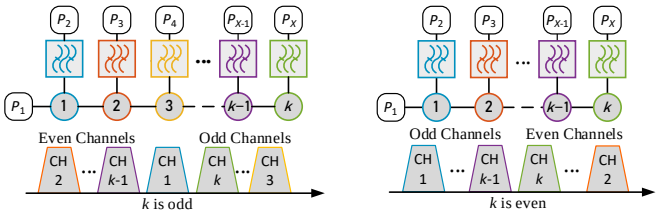

(a) (b)

Fig. 18. Channel extension scheme for the manifold multiplexer.

highly related to the number of variables in the optimization. For this multiplexer, the time cost is within 30 minutes. The optimized matrix is given in Table IV. The corresponding S-parameter responses are shown in Fig. 17.

From the two successful coupling-matrix syntheses, a general channel extension and frequency allocation scheme can be derived for the resonant manifold multiplexers with k (k≥3) channels, as illustrated in Fig. 18. With this scheme, the multiplexer can be split into multiple sub-circuits (filters and diplexers) for preparing the starting coupling values. The whole coupling matrix for the multiplexer can be obtained by using the GACMS optimization framework [23]. Robust convergence has been exhibited. It should be noted that for other frequency allocations as listed in the Appendix, the extension schemes will not be the same but very similar. For the integrality of the paper, this is not elaborated.

B. *Physical realization for the 20th-order multiplexer*

Again, the real coupling values and resonator frequencies are denormalized and calculated based on (6)-(8). The structural configuration of the multiplexer is shown in Fig. 19. All the resonators are coupled via inductive irises. In this structure, d_1, d_2 … d_{19} denote the coupling iris widths between resonators. q_1, …, q_6 denote the input/output coupling iris widths. l_1, …, l_{20} represent the lengths of resonators.

The initial dimensions are extracted based on the classical dimensioning method [24]-[25]. Due to mutual interference between channels and a large number of design variables in the multiplexer structure, it is almost impossible to directly optimize the structure as a whole. In this case, a step-tune method [28]-[29] has been adopted. The optimization starts from the port away from the manifold in each branch. Resonators are added one by one to execute the optimization until the couplings to the resonant manifold are optimized. The optimization goal is to match the simulated responses to the ideal responses from the sub-coupling-matrix. In each optimization step, only the length and the output coupling of the added resonator are altered. Therefore, the optimization is fast to converge. After the optimization of all the branches, a similar progressive optimization for the resonant manifold is performed. This step tune approach ensures more robust convergence in the optimization. Fig. 20 shows the optimized solution, comparing with the S-parameter responses calculated by coupling matrix. A very good agreement between simulation and theory has been achieved. All 20 reflection zeros are clearly visible.

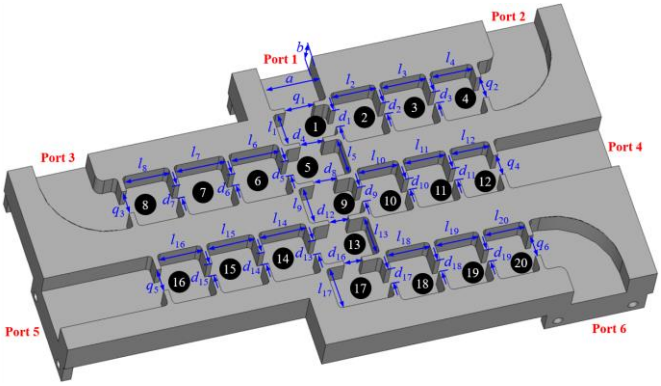

Fig. 19. Structural configuration of the 5-channel resonant manifold multiplexer. a = 22.86, b =10.16, l_1 = 14.18, l_2 = 18.20, l_3 = 18.73, l_4 = 17.37, l_5 = 15.88, l_6 = 20.24, l_7 = 20.47, l_8 = 18.98, l_9 = 16.16, l_{10} = 17.03, l_{11} = 17.28, l_{12} = 16.12, l_{13} = 16.96, l_{14} = 19.15, l_{15} = 19.37, l_{16} = 18.01, l_{17} = 17.97, l_{18} = 17.93, l_{19} = 18.09, l_{20} = 16.90, d_1 = 7.59, d_2 = 4.91, d_3 = 5.35, d_4 = 9.85, d_5 = 6.67, d_6 = 5.26, d_7 = 5.71, d_8 = 9.53, d_9 = 6.43, d_{10} = 4.79, d_{11} = 5.11, d_{12} = 8.33, d_{13} = 6.41, d_{14} = 5.09, d_{15} = 5.46, d_{16} = 7.48, d_{17} = 6.43, d_{18} =5.07, d_{19} = 5.28, q_1 = 12.43 q_2 = 9.56, q_3 = 10.02, q_4 = 9.01, q_5 = 9.65, q_6 = 9.19. Unit: millimeters. The thicknesses of all the irises are 2 mm. The radiuses of all the rounded corners are 1.5 mm.

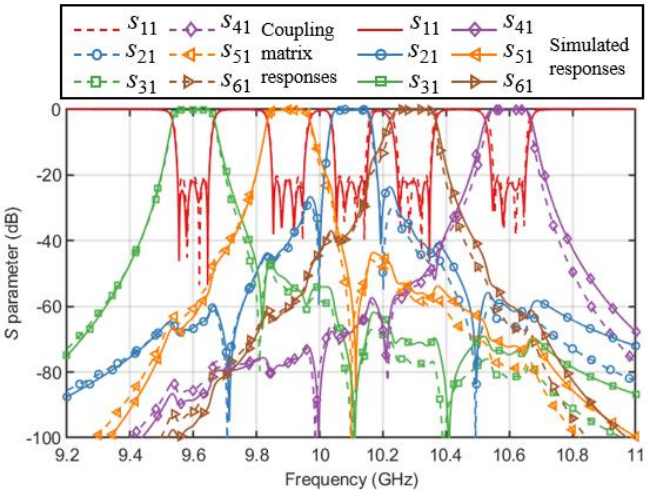

Fig. 20. Comparison of the S-parameter responses between the coupling matrix and simulation.

V. Fabrication and Measurements

A. *Triplexer*

The triplexer is machined from aluminum shown in Fig. 21. It is cut along the top edges of the resonators. This cutting plane is prone to leakage so good contact is essential. Two parts of the triplexer are assembled and tightened together by metal screws. No tuning is applied.

The triplexer is measured by using a Keysight E5071C network analyzer. The measured S-parameter responses comparing with the simulation results are shown in Fig. 22. A good agreement has been achieved between them. The insertion losses on average for the three channels are 0.96 dB, 1.33 dB and 1.31 dB, respectively. The simulated insertion losses are about 0.7dB. The higher-than-expected insertion loss is believed to be a result of contact losses from the unfavorable split plane.

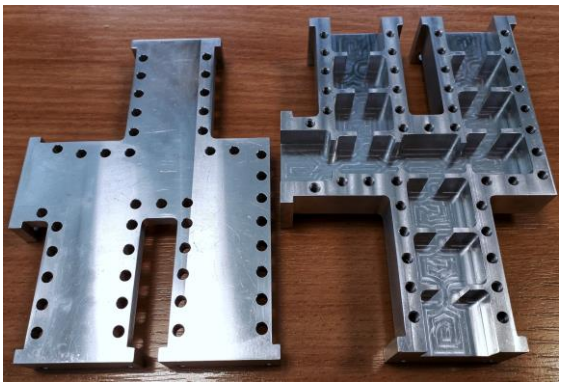

Fig. 21. Photograph of the fabricated resonant manifold triplexer.

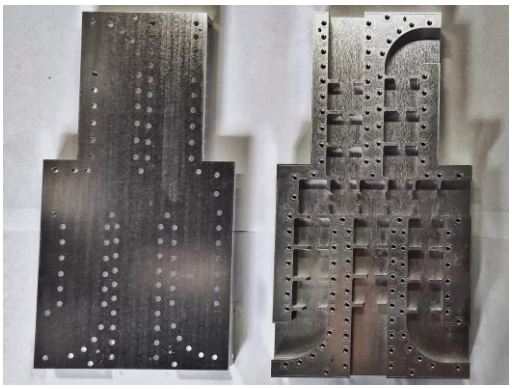

Fig. 23. Photograph of the fabricated 5-channel resonant manifold multiplexer

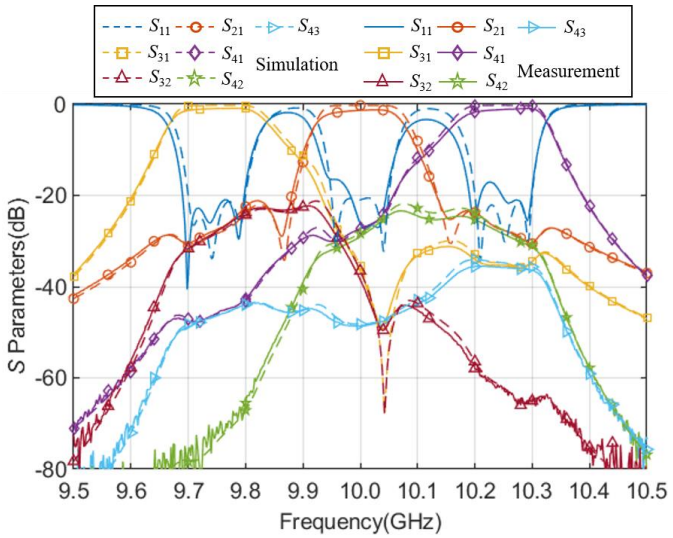

Fig. 22. Measured S-parameter responses of the triplexer in comparison with the simulated results.

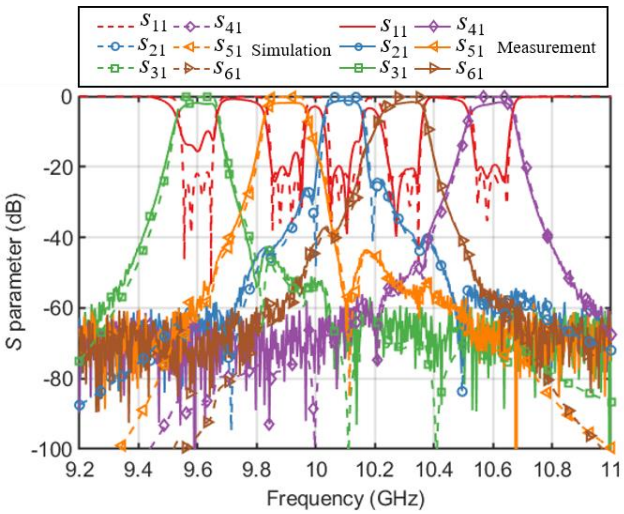

Fig. 24. Measured S-parameter responses of the 5-channel resonant manifold multiplexer comparing with the simulated results.

B. 5-channel multiplexer

The 5-channel multiplexer is fabricated using aluminum with a natural oxidation process on the surface as shown in Fig. 23. The measured S-parameter responses, in comparison with simulations, are illustrated in Fig. 24. Again, reasonably good agreement has been achieved between them without applying any tuning. The insertion losses on average for the five channels are 1.89 dB, 1.86 dB, 1.22 dB, 1.87 dB, and 2.11 dB, respectively. The simulated insertion loss obtained by using CST simulation is around 0.7dB.

The measured losses for the two multiplexers are higher than simulation results and uneven for different channels. This is mainly attributed to the H-plane cut design. As mentioned before, this cut plane is prone to contact losses. The large contact areas of the multiplexer exacerbated the imperfect connection between the two pieces. This is supported by modelling. The 5-channel multiplexer is re-simulated with a thin layer of air added between the cap and multiplexer body. It has been found the re-simulation responses match the measurement responses much better when the air gap is assumed to be 3.5 μm, which is plausible, as shown in Fig. 25. In practice, an E-plane cut structure, which is entirely possible with the resonant manifold topology, can be used and better performance is expected.

VI. Conclusion

This article presented a novel multiplexer configuration based on a resonant manifold structure. This configuration has a more compact footprint than the conventional manifold multiplexer. The proposed multiplexer has been designed based on the coupling matrix synthesis method. A frequency allocation scheme was proposed for multiplexers with different numbers of channels. The coupling matrix for the multiplexers can be efficiently obtained by using the GACMS optimization method. Two waveguide multiplexers operating at X-band are prototyped. The measurement results for both devices have shown good agreement with the corresponding simulations. This strongly validates the realizability of the proposed new multiplexer structure and the proposed design method. The resonant manifold offers a more compact multiplexer topology. The demonstrated design concept is not restricted to waveguide resonators and can be applied more widely. It may find applications in mobile base stations or satellite payloads.

However, the resonant manifold multiplexer has a limitation in its isolation performance as compared with conventional manifold multiplexers. One way to address this is to increase the order of channel filters and appropriately assign

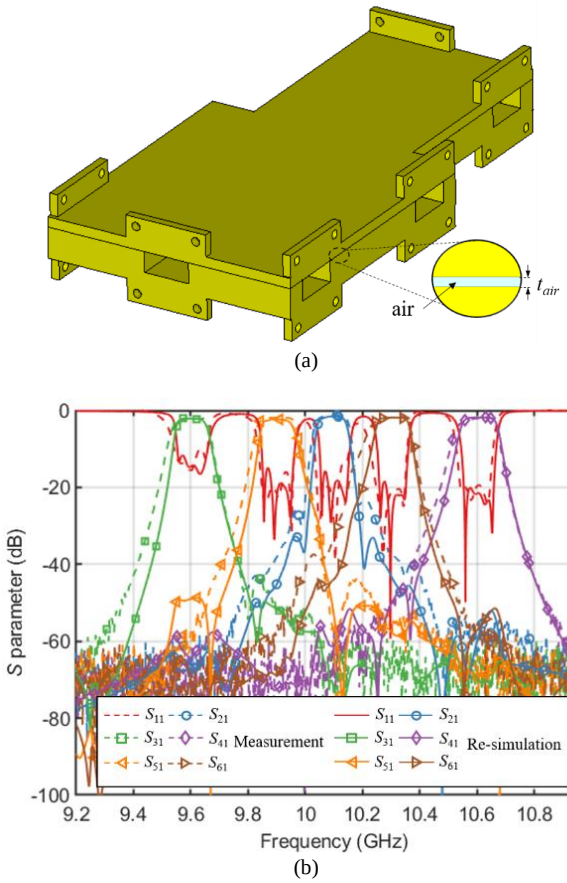

Fig. 25. Investigation on the effect of poor contact of the 5-channel multiplexer. (a) The modified model with an air gap. (b) Simulation responses showing a much better agreement with the measurement responses when air layer thickness equals to t_{air} = 3.5 μm.

transmission zeros by using cross-coupling or extracted pole structures in the branches. A balance must be made here so that the additional resonators will not dimmish the size reduction brought by the removal of the large waveguide manifold junction.

APPENDIX

The triplexer topology with different frequency allocation schemes can result in different filtering responses. The combinations of frequency allocations can be put into three categories and demonstrated here. Scheme 2 is chosen for the final design. Note that all the coupling matrix optimization processes utilize the same topology separation scheme to prepare the initial coupling values, as shown in Fig. 2. In addition, the same objective function, as expressed in (9), is used.

A. Frequency allocation scheme 1: (a) CH_1-CH_2-CH_3 or (b) CH_3-CH_2-CH_1

In this scheme, the topological channels are assigned with frequencies sequentially either from low to high or the other way around. The S-parameter responses after optimization are shown in Fig. 26. The corresponding coupling values are listed in Table V and VI. It can be observed that although the return loss responses are satisfactory, the transmission responses exhibit strong interference between the channels.

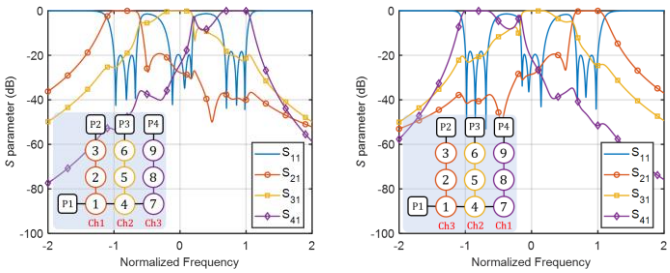

Fig. 26. S-parameter responses for the resonant manifold triplexer. (a) Frequency allocation scheme 1(a); (b) Frequency allocation scheme 1(b).

TABLE V
OPTIMIZED COUPLING VALUES WITH ALLOCATION SCHEME 1(A)

m(1, 2)	*m*(2, 3)	*m*(1, 4)	*m*(4, 5)	*m*(5, 6)	*m*(4, 7)	*m*(7, 8)
0.2989	0.1765	0.6936	0.4099	0.2204	0.2877	0.3019
m(8, 9)	*m*(1, 1)	*m*(2, 2)	*m*(3, 3)	*m*(4, 4)	*m*(5, 5)	*m*(6, 6)
0.2125	-0.0373	-0.8327	-0.8440	0.1440	-0.0877	-0.0419
m(7, 7)	*m*(8, 8)	*m*(9, 9)	*m*(1, *P*1)	*m*(3, *P*2)	*m*(6, *P*3)	*m*(9, *P*4)
0.5182	0.5968	0.7917	0.7662	0.4478	0.4424	0.4368

TABLE VI
OPTIMIZED COUPLING VALUES WITH ALLOCATION SCHEME 1(B)

m(1, 2)	*m*(2, 3)	*m*(1, 4)	*m*(4, 5)	*m*(5, 6)	*m*(4, 7)	*m*(7, 8)
0.2912	0.1679	0.6979	0.4111	0.2221	0.2871	0.3136
m(8, 9)	*m*(1, 1)	*m*(2, 2)	*m*(3, 3)	*m*(4, 4)	*m*(5, 5)	*m*(6, 6)
0.2317	0.0268	0.8413	0.8519	-0.1395	0.1232	0.0749
m(7, 7)	*m*(8, 8)	*m*(9, 9)	*m*(1, *P*1)	*m*(3, *P*2)	*m*(6, *P*3)	*m*(9, *P*4)
-0.5242	-0.5569	-0.7732	0.7662	0.4368	0.4424	0.4478

B. Frequency allocation scheme 2: (a) CH_2-CH_1-CH_3 or (b) CH_2-CH_3-CH_1

In this scheme, the first topological channel is assigned with the middle channel frequency, where the following two are assigned with the two bands on either side, as shown in Fig. 27 together with the S-parameter responses from the optimized coupling matrix. The coupling values are listed in Table VII and VIII. The filtering responses exhibit reasonable isolation performance. The transmission zeros appear at the appropriate place in the guard bands. This scheme is selected in this paper, consistent with the channel extension scheme proposed in Fig. 18.

C. Frequency allocation scheme 3: (a) CH_1-CH_3-CH_2 or (b) CH_3-CH_1-CH_2

This scheme is similar to Scheme 2 but the last topological channel, rather than the first, is assigned with the middle band frequency, as shown in Fig. 28. The optimized coupling values are listed in Table IX and X. The filtering responses broadly match those from Scheme 2 but with slightly higher asymmetry.

D. Channel allocation guideline

As a design guideline, for a multiplexer with an odd number of channels, both Scheme 2 and 3 can be considered for similar performance. One can make a further selection based on the physical constraint of the layout and any specific isolation or rejection requirement. It should also be noted that the required coupling levels are similar for both schemes. For multiplexers with an even number of channels, the scheme shown in Fig.

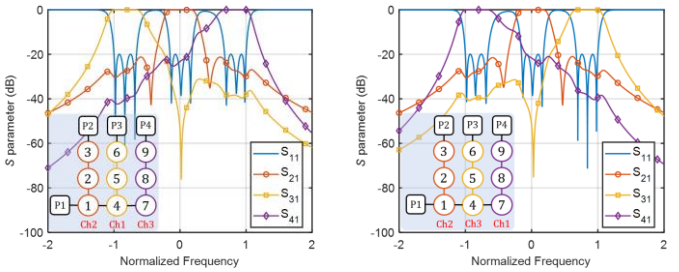

(a) (b)

Fig. 27. S-parameter responses for the resonant manifold triplexer. (a) Frequency allocation scheme 2(a); (b) Frequency allocation scheme 2(b).

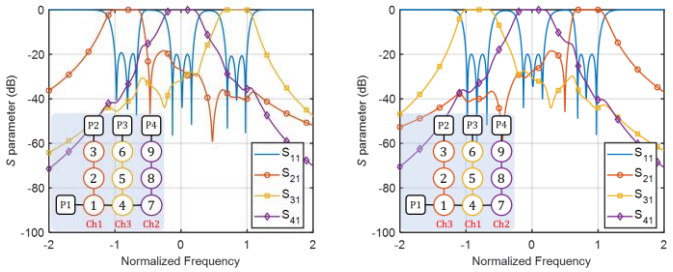

(a) (b)

Fig. 28. S-parameter responses for the resonant manifold triplexer. (a)Frequency allocation scheme 3(a). (b) Frequency allocation scheme 3(b).

TABLE. VII
OPTIMIZED COUPLING VALUES WITH ALLOCATION SCHEME 2(A)

m(1, 2)	*m*(2, 3)	*m*(1, 4)	*m*(4, 5)	*m*(5, 6)	*m*(4, 7)	*m*(7, 8)
0.2982	0.1706	0.7113	0.2346	0.1780	0.5616	0.2957
m(8, 9)	*m*(1, 1)	*m*(2, 2)	*m*(3, 3)	*m*(4, 4)	*m*(5, 5)	*m*(6, 6)
0.1838	0.0042	0.0138	0.0138	−0.0127	−0.7970	−0.8240
m(7, 7)	*m*(8, 8)	*m*(9, 9)	*m*(1, *P*1)	*m*(3, *P*2)	*m*(6, *P*3)	*m*(9, *P*4)
0.1533	0.7163	0.8154	0.7662	0.4424	0.4478	0.4368

TABLE IX
OPTIMIZED COUPLING VALUES WITH ALLOCATION SCHEME 3(A)

m(1, 2)	*m*(2, 3)	*m*(1, 4)	*m*(4, 5)	*m*(5, 6)	*m*(4, 7)	*m*(7, 8)
0.3035	0.1765	0.7096	0.2145	0.1688	0.4514	0.1958
m(8, 9)	*m*(1, 1)	*m*(2, 2)	*m*(3, 3)	*m*(4, 4)	*m*(5, 5)	*m*(6, 6)
0.1772	-0.0068	-0.8309	-0.8412	0.1336	0.8127	0.8341
m(7, 7)	*m*(8, 8)	*m*(9, 9)	*m*(1, *P*1)	*m*(3,*P*2)	*m*(6,*P*3)	*m*(9,*P*4)
-0.0170	0.0059	0.0129	0.7662	0.4478	0.4368	0.4424

TABLE. VIII
OPTIMIZED COUPLING VALUES WITH ALLOCATION SCHEME 2(B)

m(1, 2)	*m*(2, 3)	*m*(1, 4)	*m*(4, 5)	*m*(5, 6)	*m*(4, 7)	*m*(7, 8)
0.2980	0.1706	0.7108	0.2254	0.1692	0.5658	0.3177
m(8, 9)	*m*(1, 1)	*m*(2, 2)	*m*(3, 3)	*m*(4, 4)	*m*(5, 5)	*m*(6, 6)
0.1946	-0.0149	0.0152	0.0152	0.0082	0.8082	0.8328
m(7, 7)	*m*(8, 8)	*m*(9, 9)	*m*(1, *P*1)	*m*(3, *P*2)	*m*(6, *P*3)	*m*(9, *P*4)
-0.1201	-0.6923	-0.8049	0.7662	0.4424	0.4368	0.4478

TABLE X
OPTIMIZED COUPLING VALUES WITH ALLOCATION SCHEME 3(B)

m(1, 2)	*m*(2, 3)	*m*(1, 4)	*m*(4, 5)	*m*(5, 6)	*m*(4, 7)	*m*(7, 8)
0.2950	0.1688	0.7112	0.2239	0.1772	0.4516	0.1960
m(8, 9)	*m*(1, 1)	*m*(2, 2)	*m*(3, 3)	*m*(4, 4)	*m*(5, 5)	*m*(6, 6)
0.1785	-0.0057	0.8384	0.8499	-0.1297	-0.8017	-0.8247
m(7, 7)	*m*(8, 8)	*m*(9, 9)	*m*(1, *P*1)	*m*(3, *P*2)	*m*(6, *P*3)	*m*(9, *P*4)
0.0596	0.0266	0.0174	0.7662	0.4368	0.4478	0.4424

18(b) is recommended, where the consecutive pair of topological channels can be assigned with two symmetrically located frequency channels. The coupling matrices for all the schemes can be effectively synthesized by using the proposed optimization method. A general coupling matrix synthesis procedure is given in the following.

Step 1: Transform the frequency specifications into normalized frequency channels.

Step 2: If the number of channels is even, jump to Step 3. If the number of channels is odd, assign the middle-frequency channel to the first topological channel, such as the CH1 shown in Fig. 18 (a).

Step 3: Every two frequency channels located at two outer sides are assigned to the following every consecutive pair of topological channels, as shown in Fig. 18 (a) and (b).

Step 4: Divide the multiplexer into multiple sub-circuits, including a filter and multiple diplexers.

Step 5: Synthesis of the sub-circuits using the allocated frequency specifications in Step 2 and 3.

Step 6: Take the coupling values obtained in Step 5 as the starting point. Optimize the coupling matrix of the multiplexer using the GACMS method [23].

Step 7: Transform the optimal coupling matrix into the real frequency domain.

REFERENCES

[1] R. J. Cameron, C. M. Kudsia, and R. R. Mansour, "Multiplexer Theory and Design," *Microwave Filters for Communication Systems: Fundamentals, Design, and Applications*, Wiley, 2018, pp.569-608, ch18.

[2] G. Macchiarella and S. Tamiazzo, "Synthesis of Star-junction Multiplexers," *IEEE Trans. Microw. Theory Techn.*, vol. 58, no. 12, pp. 3732-3741, Dec. 2010.

[3] R. I. Cameron and M. Yu, "Design of Manifold-coupled Multiplexers," *IEEE Microw. Mag.*, vol. 8, no. 5, pp. 46-59, Oct. 2007.

[4] C. Kudsia, R. Cameron, and W.-C. Tang, "Innovations in Microwave Filters and Multiplexing Networks for Communications Satellite Systems," *IEEE Trans. Microw. Theory Techn.*, vol. 40, no. 6, pp. 1133-1149, Jun. 1992.

[5] S. Cogollos, P. Soto, V. E. Boria, M. Guglielmi, M. Brumos, B. Gimeno, and D. Raboso, "Efficient Design of Waveguide Manifold Multiplexers Based on Low-Order EM Distributed Models," *IEEE Trans. Microw. Theory Techn.*, vol. 63, no. 8, pp. 2540-2549, Aug. 2015.

[6] P. Zhao and K. Wu, "An Iterative and Analytical Approach to Optimal Synthesis of a Multiplexer with a Star-Junction," *IEEE Trans. Microw. Theory Techn.*, vol. 62, no. 12, pp. 3362-3369, Dec. 2014.

[7] G. Macchiarella and S. Tamiazzo, "Novel Approach to the Synthesis of Microwave Duplexers," *IEEE Trans. Microw. Theory Tech.*, vol. 54, no. 12, pp. 4281-4290, Dec. 2006.

[8] G. Macchiarella and S. Tamiazzo, "Design of Triplexer Combiners for Base Stations of Mobile Communications," *IEEE MTT-S Int. Microw. Symp. Dig.*, Anheim, CA, May. 2010, pp. 429–432.

[9] R. V. Snyder, A. Mortazawi, I. Hunter, S. Bastioli, G. Macchiarella, and K. Wu, "Present and Future Trends in Filters and Multiplexers," *IEEE Trans. Microw. Theory Tech.*, vol. 63, no. 10, pp. 3324-3360, Oct. 2015.

[10] A. Morini, G. Venanzoni, M. Farina, and M. Villa, "A Method for Fast and Reliable Analysis and Optimization of Side-Coupled Cavity Filters and Multiplexers," *IEEE Trans. Microw. Theory Techn.*, vol. 66, no. 8, pp. 3847-3856, Aug. 2018.

[11] M. Ismail, D. Smith, A. Panariello, Y. Wang, and M. Yu, "EM-based Design of Large-scale Dielectric-resonator Filters and Multiplexers by Space Mapping," *IEEE Trans. Microw. Theory Techn.*, vol. 52, no. 1, pp. 386–392, Jan. 2004.

[12] M. Yu and Y. Wang, "Synthesis and Beyond," *IEEE Microw. Mag.*, vol. 12, no. 6, pp. 62–76, Oct. 2011.

[13] M. Ismail, Y. Wang, and M. Yu, "Advanced Design and Optimization of Large-scale Microwave Devices," *IEEE MTT-S Int. Microw. Symp. Dig.*, Jun. 2012, pp. 1–3.

[14] Z. C. Hao, X. P. Huo, W. Q. Ding, and W. Hong, "Efficient Design of Compact Contiguous-channel SIW Multiplexers using the Space Mapping Method," *IEEE Trans. Microw. Theory Techn.*, vol. 63, no. 11, pp. 3651–3662, Nov. 2015.
[15] X. Shang, Y. Wang, W. Xia, and M. J. Lancaster, "Novel Multiplexer Topologies Based on All-Resonator Structures," *IEEE Trans. Microw. Theory Techn.*, vol. 61, no. 11, pp. 3838-3845, Nov. 2013.
[16] T. Skaik, M. Lancaster, M. Ke, and Y. Wang, "A Micromachined WR-3 Band Waveguide Diplexer based on Coupled Resonator Structures," *2011 41st European Microwave Conference (EuMC)*, Oct. 2011, pp. 770-773.
[17] Y. Wu, Y. Wang and E. A. Ogbodo, "Microstrip Wideband Diplexer with Narrow Guard Band based on All-resonator Structures," *2016 46th European Microwave Conference (EuMC)*, Oct. 2016, pp. 1163-1166.
[18] R. Wang, J. Xu, M.-Y. Wang, and Y.-L. Dong, "Synthesis of Microwave Resonator Diplexers using Linear Frequency Transformation and Optimization," *Progress In Electromagnetics Research*, vol. 124, pp. 441-456, Feb. 2012.
[19] I. Llamas-Garro, F. Mira, P. Zheng, Z. Liu, L. Wu, and Y. Wang, "All-resonator based LTCC Diplexer using Substrate-integrated-waveguides," *Electron. Lett.*, vol. 53, no. 21, pp. 1410-1412, Oct. 2017.
[20] W. Xia, X. Shang, and M. J. Lancaster, "All-resonator-based Waveguide Diplexer with Cross-couplings," *Electron. Lett.*, vol. 50, no. 25, pp. 1948-1950, Dec. 2014.
[21] T. F. Skaik, M. J. Lancaster, and F. Huang, "Synthesis of Multiple Output Coupled Resonator Circuits using Coupling Matrix Optimisation," *IET Microw. Antennas Propag.*, vol. 5, no. 9, pp. 1081-1088, Jul. 2011.
[22] B. Liu, H. Yang, and M. J. Lancaster, "Synthesis of Coupling Matrix for Diplexers Based on a Self-Adaptive Differential Evolution Algorithm," *IEEE Trans. Microw. Theory Techn.*, vol. 66, no. 2, pp. 813-821, Feb. 2018.
[23] Y. Yu, B. Liu, Y. Wang, M. J. Lancaster, and Q. S. Cheng, "A General Coupling Matrix Synthesis Method for All-Resonator Diplexers and Multiplexers," *IEEE Trans. Microw. Theory Techn.*, vol. 68, no. 3, pp. 987-999, Mar. 2020.
[24] J. -S. G. Hong and M. J. Lancaster, *Microstrip Filters for RF/Microwave Application*, vol. 167. Hoboken, NJ, USA: Wiley, 2004.
[25] R. J. Cameron, C. M. Kudsia, and R. R. Mansour, "Design and Physical Realization of Coupled Resonator Filters," *Microwave Filters for Communication Systems: Fundamentals, Design, and Applications*. Hoboken, NJ, USA: Wiley, 2018, pp.457-484, ch14.
[26] S. Llorente-Romano and M. Salazar-Palma, "Implementation of Extracted Pole Filters in Rectangular Waveguide," *2014 44th European Microwave Conference*, Oct. 2014, pp. 616-619.
[27] CST Studio Suite – EM Simulation Software. [Online]. Available: http:// https://www.3ds.com/products-services/simulia/products/cst-studio-suit.
[28] M. Guglielmi, "Simple CAD Procedure for Microwave Filters and Multiplexers," *IEEE Trans. Microw. Theory Techn.*, vol. 42, no. 7, pp. 1347-1352, Jul. 1994.
[29] X. Shang, W. Xia, and M. J. Lancaster, "The design of waveguide filters based on cross-coupled resonators," *Microw. Opt. Technol. Lett.*, vol. 56, pp. 3-8, Nov. 2014.
[30] D. Swanson and G. Macchiarella, "Microwave filter design by synthesis and optimization," *IEEE Microw. Mag.*, vol. 8, no. 2, pp. 55-69, Apr. 2007.
[31] R. V. Snyder, G. Macchiarella, S. Bastioli, and C. Tomassoni, "Emerging Trends in Techniques and Technology as Applied to Filter Design," *IEEE J. Microwaves*, vol. 1, no. 1, pp. 317-344, Jan. 2021.
[32] J. Bornemann, U. Rosenberg, S. Amari, and R. Vahldieck, "Tolerance analysis of bypass-, cross- and direct-coupled rectangular waveguide band-pass filters," *Proc. Inst. Elect. Eng.-Microw. Antennas Propag.*, vol. 152, no. 3, pp. 167–170, Jun. 2005.
[33] Z. Zhang, H. Chen, Y. Yu, F. Jiang, and Q. S. Cheng, "Yield-Constrained Optimization Design Using Polynomial Chaos for Microwave Filters," *IEEE Access*, vol. 9, pp. 22408-22416, Jan. 2021.